

# Generative Adversarial Networks for Labeled Data Creation for Structural Monitoring and Damage Detection

Furkan Luleci<sup>1</sup>; F. Necati Catbas<sup>2\*</sup>, Ph.D., P.E.; Onur Avci<sup>3</sup>, Ph.D., P.E.

<sup>1</sup>Doctoral Student, Department of Civil, Environmental, and Construction Engineering, University of Central Florida, Orlando, FL, 32816, USA (Email: [furkanluleci@Knights.ucf.edu](mailto:furkanluleci@Knights.ucf.edu))

<sup>2</sup>Professor, Department of Civil, Environmental, and Construction Engineering, University of Central Florida, Orlando, FL, 32816, USA (Email: [catbas@ucf.edu](mailto:catbas@ucf.edu))

<sup>3</sup> Research Assistant Professor, Civil, Construction, and Environmental Engineering, Iowa State University, Ames, IA, 50011, USA (Email: [oavci@iastate.edu](mailto:oavci@iastate.edu))

**Abstract:** There has been a drastic progression in the field of Data Science in the last few decades and other disciplines have been continuously benefitting from it. Structural Health Monitoring (SHM) is one of those fields that use Artificial Intelligence (AI) such as Machine Learning (ML) and Deep Learning (DL) algorithms for condition assessment of civil structures based on the collected data. The ML and DL methods require plenty of data for training procedures; however, in SHM, data collection from civil structures is very exhaustive; particularly getting useful data (damage associated data) can be very challenging. The objective of this study is to address the data scarcity problem for damage detection. This paper first presents 1-D Wasserstein Deep Convolutional Generative Adversarial Networks using Gradient Penalty (1-D WDCGAN-GP) for synthetic labelled vibration data generation. Then, implements structural damage detection on different levels of synthetically enhanced raw vibration datasets by using 1-D Deep Convolutional Neural Network (1-D DCNN). The damage detection results show that the 1-D WDCGAN-GP can be successfully utilized to tackle data scarcity in vibration-based damage diagnostics of civil structures.

**Keywords:** Structural Health Monitoring (SHM), Structural Damage Detection, 1-D Deep Convolutional Neural Networks (1-D DCNN), 1-D Generative Adversarial Networks (1-D GAN), Wasserstein Generative Adversarial Networks with Gradient Penalty (WGAN-GP)

## 1) Introduction and background on Structural Damage Detection (SDD)

Man-made or environmental stressors tend to decrease the remaining useful lives of civil structures. As the ageing civil infrastructures are getting more vulnerable to such impacts, more comprehensive assessment and effective health management plans are needed to improve the life cycle of structures.

The typical workflow to monitor and assess an existing civil structure starts with collecting operational data with sensors such as accelerometers, strain gauges, potentiometers, fiber optic sensors or load cells. As the following step, the data is pre-processed and analyzed to perform damage identification based on the changes in the structural parameters (stiffness, mass, damping, etc.) or in the raw data to identify structural defects (crack, delamination, corrosion, bolt-loosening, spalling, etc.) The common practice of diagnosing damage in SHM is via accelerometers since it is advantageous over other methods [1].

Applications of damage detection can be divided into local methods and global methods. Local methods include Non-Destructive Testing (NDT) and some of the camera sensing techniques like Infrared Thermography (IR), Digital Image Correlation (DIC). Global methods (vibration-based) include the analysis of collected data parametrically (using a physical model like FEA program or non-physical

model like system identification methods) or nonparametrically (extracting meaningful features from the collected raw data – in other words damage detection without relating to structure's parameters) [2]. Additionally, via advanced Computer Vision methods, damage detection can be performed at local and global levels [3].

Numerous studies have been reported for structural damage detection of civil structures: [4] demonstrated that the boundary conditions of a structure can be determined by looking at its deflection profile which the authors obtained using test data from a laboratory grid structure. [5] detected the presence and quantified the damage by extracting the modal properties via Natural eXcitation Technique (NeXT) and Eigenvalue Realization Algorithm (ERA) from the collected vibration data of transmission towers. [6] utilized Auto-Regressive Moving Average (ARMA) and then Gaussian Mixture Model (GMM) to first extract the features and to classify them by using Mahalanobis distance metric on the collected vibration data. The authors successfully identified undamaged and damaged datasets. [7] utilized Auto-Regressive eXogenous output (ARX) to extract and then implemented clustering technique to classify the undamaged and damaged cases in the collected vibration data from a grid structure. [8] focused on the vibration datasets to determine outliers by using Genetic Algorithm (GA) based clustering on decision boundary analysis (GADBA). One of the common details in the above-mentioned parametric and nonparametric vibration-based damage detection studies is that the amount of data is not prominent on the success of the used methods.

The ML and DL methods require a substantial amount of data samples to train the algorithms, especially DL algorithms yield outstanding results on more and more data [9]. With superior performance on feature extraction, classification, regression, and clustering, ML and DL methods have been widely accepted in civil SHM for both parametric and nonparametric vibration-based damage detection. It is observed that Artificial Neural Networks (ANN) is the most used one in ensembled other algorithms and Support Vector Machine (SVM) comes in second for SHM applications. Some of the introduced studies are [10–17]. When using an ML model for nonparametric damage detection purposes, features from the raw data need to be extracted by using some of the computational tools such as Principal Component Analysis (PCA) or Autoregressive (AR) models, which may cause computational complexity along with other limitations [2]. On the other hand, the DL algorithms can make highly accurate predictions by learning the features directly in the raw data without having to need any extracting tools. In other words, with a correctly built model and the right training process, DL algorithms can show superior performance over ML methods. In the civil SHM area, a few unsupervised DL methods, which are mostly Autoencoders [18–20] and some supervised DL methods which are mostly Convolutional Neural Networks [21–25] are presented.

## **1.2) Objective and Scope of this work**

Data collection in SHM of civil structures can be exhaustive, challenging, and expensive. Requesting permission from authorities to install expensive and laborious SHM systems, requesting traffic closures, etc. and needing skilled experts on the field are just some of the mentioned exhaustive tasks. Considering that only a very few civil structures have permanent SHM systems in the world, it is hard to predict the damage state on the remaining structures that do not have SHM data or very limited SHM data. As a result of these challenges, the opportunity to find useful data (damage associated data, *labelled data*) for the civil structure is rare. This creates a class imbalance complication to implement vibration-based methods with AI algorithms for structural assessment purposes. The effect of class imbalance on classification performance of DL model is detrimental and the impact increases when the ratio of imbalance in dataset increases. One solution can be oversampling the already existing dataset: in other words, increasing the amount of sampled data with exact copies. Yet, in this method, the AI model does not learn the variation of the damage-associated data, but only utilized the provided exact copies of the input, which can cause the model to overfit the training dataset. Another solution can be using random

transformation methods to enhance/augment the data which requires manual work before applying it to data. Since each dataset has its own characteristics and there are diverse amounts of data, not every transformation is applicable to every dataset. Also, random transformations unintentionally change the distribution of the data [26]. Another solution can be building a Finite Element (FE) model to produce displacement, stress, or acceleration data to tackle the data scarcity by analyzing the structure under similar damage scenarios simulated in the FE model. However, this method is not reliable compared to collecting actual data from a real structure as it is quite difficult to simulate the damage cases comprehensively in an FE model [27]. These challenges can yield inaccurate results for DL models when used for vibration-based damage detection. The recent novel AI methods such as GAN have proved state-of-the-art results for generating data samples and have superior skills for learning the data domain.

While the data scarcity hinders the utilization of the ML and DL algorithms, this study presents using 1-D Generative Adversarial Networks (1-D GAN) in structural damage detection. The GAN is utilized to generate data samples to train the 1-D Deep Convolutional Neural Networks (1-D DCNN) to perform nonparametrically (directly on raw data) vibration-based damage detection on a laboratory structure. The scope of the presented work is a good fit for representing realistic scenarios that could be encountered during the operations of civil structures. For instance, when the existing dataset is very scarce to run a DL model to perform damage detection, GAN can be employed to enhance/augment the training datasets with synthetic samples of data. The introduced methodology in this paper will pave the way for additional ML and DL algorithms to be integrated with damage detection on civil structures.

The objective of this study is to investigate the integrated use of 1-D GAN and 1-D DCNN to address the data scarcity problem for nonparametric vibration-based structural damage detection (level-I damage diagnostics). Firstly, a state-of-the-art GAN variant 1-D Wasserstein Deep Convolutional Generative Adversarial Networks using Gradient Penalty (1-D WDCGAN-GP) is employed for synthetic labelled vibration data generation to enhance the training data. Then, training the 1-D DCNN with the synthetically enhanced data for structural damage detection on the unseen raw vibration data to demonstrate the applicability of the performed data enhancement for nonparametric damage detection.

### 1.3) Existing work on Generative Adversarial Networks

[28] proposed an unsupervised DL network that contains two distinct networks: a generative network,  $G_\theta$ , that captures the given randomly distributed data,  $z$ , and aims to maximize the probability of the output it generates,  $G_\theta(z)$ , very alike to the training dataset,  $x$ , in other words, the generator tries to minimize the probability that the prediction of discriminator on generator's outputs is not real. The discriminative network,  $D_\phi$ , aims to maximize the likeliness of the output it gets from the generator,  $G_\theta(z)$ , is not real and from the training data,  $x$ , is real. Thus, it is thought of as a two-player game where each player is trying to trick the other. The fundamental formulation of the loss function of GAN is shown in Equation 1.

$$\min_{\theta} \max_{\phi} V(G_\theta, D_\phi) = E_{x \sim p_{data}(x)} [\log D_\phi(x)] + E_{z \sim p_z(z)} [\log(1 - D_\phi(G_\theta(z)))] \quad (1)$$

The GAN is successfully used on image-based applications and then adopted in several other applications. Among all the DL networks, training of GAN is arguably one of the most difficult ones, but it comes with a trade-off of superior generative performance. For example, reaching a convergence due to the difficulty of finding a unique solution to Nash equilibrium where the model is searching for a balance point between the two sides in the optimization, instead of finding a minimum one. Consequently, GAN experiences large oscillations in loss values which leads to an unstable training process and model performance. Occasionally, GAN suffers from mode collapse, in another word, the generator learns only some specific features in the given training data where the discriminator can be deceived. Thus, the GAN keeps producing the same data samples to trick the discriminator which reduces the creativity of the

model and diversity of the outputs. GAN also suffer from the discriminator being powerful over the generator. As a result, training the generator could fail due to vanishing gradients, hence, the discriminator does not provide enough information for the generator to learn [29, 30]. Although the mentioned drawbacks make it harder to train GAN, they are state-of-the-art generative-based models that have superior learning skills in the given data domain as demonstrated in the computer vision field. Thus, researchers focused on improving the training procedure of GAN which are discussed in the next paragraph. Also, tips, namely “hacks” are introduced in the DL community to alleviate these drawbacks and some of which are used in the presented work herein.

[31] introduced the use of convolutions in GAN (and called it **DCGAN**) after their successful adoption in computer vision applications. The authors noted that convolutions helped GAN to learn significantly better. However, to address the challenges in the training of GAN, [32] introduced GAN that uses Wasserstein distance as a loss function (**Wasserstein Generative Adversarial Networks - WGAN**) and demonstrated that it improves the training remarkably. In WGAN, the authors used “critic” over discriminator where instead of scoring the likelihood of the generated data is real or fake, it scores the output of generator as how close to the real or fake on a given image. Essentially, WGAN looks for a minimization of the distance between the produced and the training dataset distributions in the range of a real or fake distance. GAN benefited greatly from using the Wasserstein metric. It provided more stable training; the results are less sensitive to the parameters and model architecture, and the loss function is more meaningful which directly relates to the quality of generated images. WGAN uses weight clipping to enforce the Lipschitz constraint on the critic to compute the Wasserstein distance; however, it causes the model to lower its learning capacity. It is also very sensitive to the selected parameters. If large weight clipping is used, it increases the computation time drastically; if the clipping is small, it could easily lead to vanishing gradients. To tackle the weight clipping problem, [33] proposed a penalization of the gradient during the training of the critic instead of using weight clipping. The authors showed that the method they introduced yields better performance than WGAN and resulted in more stable training and the authors named presented the model as **WGAN-GP (Wasserstein Generative Adversarial Networks using Gradient Penalty)**.

The computer Vision field largely benefited from using GAN on various image applications which are 2-D data. Additionally, some studies in different disciplines were successful at using GAN for 1-D data generation and data reconstruction for various purposes [34–39]. Several GAN based 1-D data generation, reconstruction, and ML classifier related studies are presented in the field of non-civil SHM [40–43]. In the civil SHM field, few studies are presented for GAN based 1-D data reconstruction [44–46]. Yet, at the time of this paper preparation, there was not any study utilizing the **WGAN** and **WGAN-GP** comprehensively to address the data scarcity issue for civil SHM, to the best information of the authors.

## 2) Framework of the study

In the proposed work, **1-D WGAN-GP** that is built on convolutions is used to generate synthetic datasets which are named “**1-D WDCGAN-GP**” in short by the authors for **One Dimensional Wasserstein Deep Convolutional Generative Adversarial Networks using Gradient Penalty**. Then, **1-D DCNN (1-D Deep Convolutional Neural Network)** is used to implement nonparametric damage detection (damage detection on raw vibration data) on the scenarios that might be encountered during an SHM of civil structures. For simplicity, in the remaining of the paper, **1-D WDCGAN-GP** and **1-D DCNN** are referred to as  $M_1$  and  $M_2$ , respectively. The rest of the paper is presented in the following order: framework of the study in section 2, the workflow of the 1-D WDCGAN-GP in section 3, and workflow of the 1-D DCNN in section 4. Summary and conclusions are presented at the end.

The vibration dataset used in this work is obtained from a study by [23] on a steel laboratory frame (Fig. 1) where they installed 30 accelerometers at 30 joints. A modal shaker random excitation is applied to the

structure and consequently 1 undamaged and 30 damaged scenarios are created at each joint separately by loosening the bolts at the steel connections between filler beams and girders. Then, at a 1024 Hz of sampling rate, the authors collected 256 seconds of vibration data with a total sample of  $256 \times 1024 = 262,144$  from each accelerometer channel dedicated to a joint (Fig. 1). The 1-D vibration arrays are named tensors and the notation used in this paper is  $n[a_{klf}]_s$  where  $k$  represents the condition such as 0 refers to the data is collected in an undamaged scenario, 1 refers to the damaged scenario,  $l$  represents the joint number (only joint 1 is used in this study) where the data is collected from based on Fig. 1, and  $f$  refers to “fake” if the tensor is generated by the  $M_1$ . Lastly,  $s$  refers to the seconds that the tensor contains, and  $n$  refers to the number of tensors. The  $n$  is featured to 1 if there is no number written. In this study, the  $s$  is only used as 1 and 256 respectively where 1 refers to “1-second” (batched from 256 seconds) and 256 refers to “256-seconds” (entire raw signal). Lastly, the PC used in this study has the following specs: 16 GB RAM DD4 2933 MHz and NVIDIA GeForce RTX 3070 8GB GDDR6 graphic card.

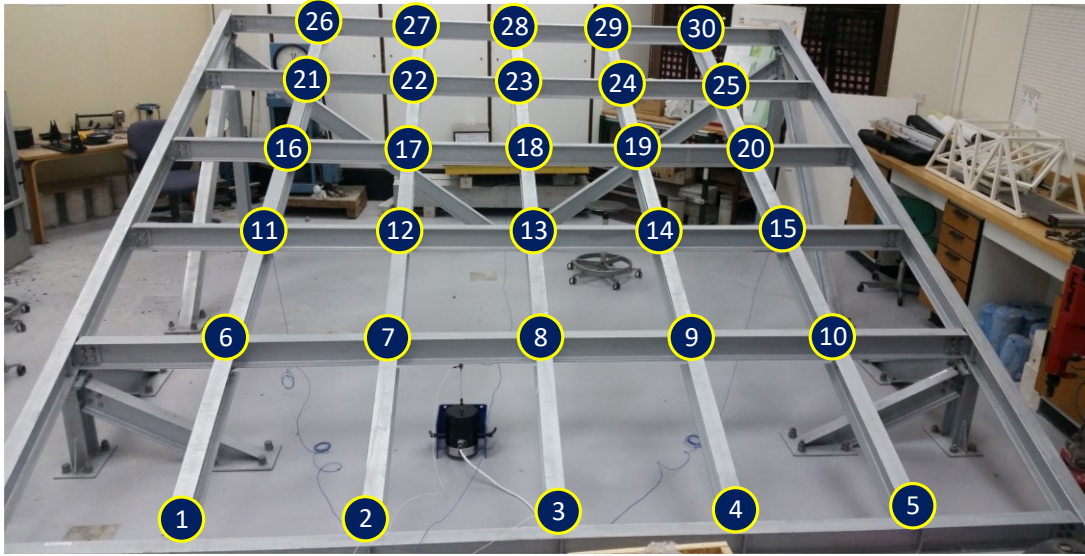


**Fig. 1.** Steel Frame Grand Simulator Structure [23]

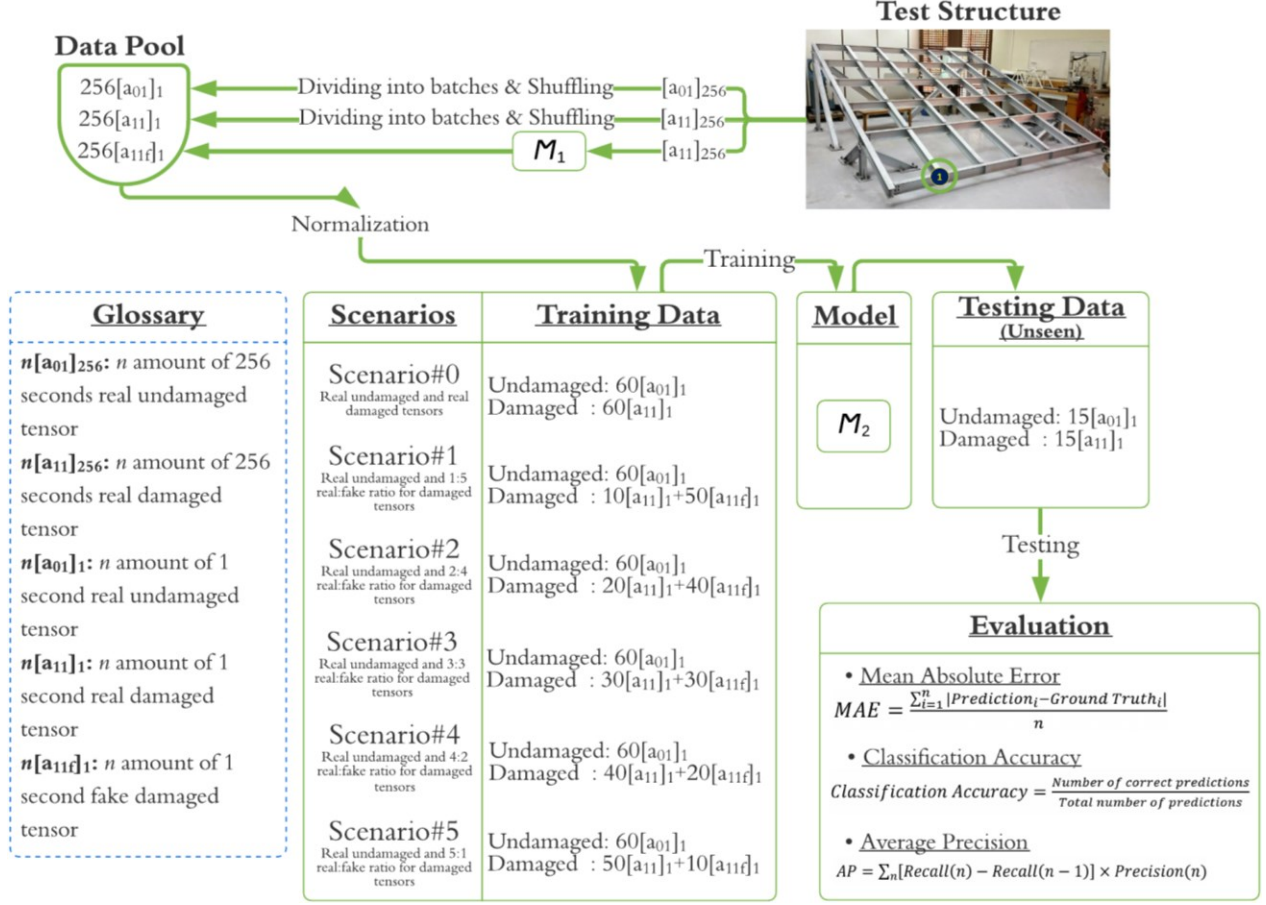


**Fig. 2.** The framework

The workflow of this study is presented in Fig. 2. First, the tensor  $[a_{11}]_{256}$ , 256 seconds (262,144 samples) real damaged tensor, is input in the  $M_1$  to generate the synthetic datasets of  $256[a_{11f}]_1$ , 256 amount of 1 second (1024 samples) fake damaged tensors. The  $[a_{01}]_{256}$ , 256 seconds (262,144 samples) real undamaged tensor, and  $[a_{11}]_{256}$  are batched into 256 amounts of 1-second tensors,  $256[a_{01}]_1$  and  $256[a_{11}]_1$ , then randomly shuffled and placed in the data pool without replacement. Two reasons why batching in shuffle mode is used: (i) to prevent any bias in the model such as learning the data in the order that is provided and (ii) to converge the training faster. A similar method is also successfully implemented and described by [21]. The authors divided the input signal into frames and randomly shuffled it. Nevertheless, the sequence of the dataset or the parameters of the vibration tensors is irrelevant because the purpose of the study is to show that GAN can tackle the data scarcity for nonparametric (directly on raw data) damage detection for civil structures. After the normalization, these tensors are passed in  $M_2$  for training and testing data for six different scenarios of which five of them includes potential real-life cases (Scenario#1-5). Note that the datasets that are used in training are not used in testing.

In Scenario#0, for benchmarking purposes with other scenarios, no synthetic data is involved, but only real tensors are used. To represent that,  $60[a_{01}]_b$  and  $60[a_{11}]_b$  for training and  $15[a_{01}]_1$  and  $15[a_{11}]_1$  tensors are used for testing. In Scenario#1 to Scenario#5, real undamaged tensors are used for both training and testing. However, the real damaged tensors are enhanced with different amounts of synthetic tensors for Scenario#1 to Scenario#5. For instance, for Scenario#1, while the undamaged class has  $60[a_{01}]_1$  (60 amount of 1 second of the real undamaged tensor), the damaged class has  $10[a_{11}]_1$  (10 amount of 1-second of the real damaged tensor) and  $50[a_{11f}]_1$  (50 amount of 1-second of the fake



damaged tensor). The same logic can be extrapolated to other scenarios as illustrated in Fig. 2. For testing  $15[a_{01}]_1$  and  $15[a_{11}]_1$  tensors are used. The reasoning behind creating the scenarios in this way is to reflect the possible scenarios that can be encountered in SHM to perform damage detection of civil structures. As previously mentioned, obtaining damage-associated datasets from large civil engineering structures is challenging; and to do damage detection via a DL model on a particular structure, it is essential to have a sufficient amount of data samples for each class (undamaged or damaged classes).

Each scenario presented in Fig. 2, from Scenario#1 to Scenario#5, shows that enough amount of tensor exists in the undamaged class, but the tensor in the damaged class is very scarce for the particular damage case. This case is most of the time true for bridge structures. The authors of this study envision that the introduced methodology can be used for bridge structures after further validated investigations and developments on the used methodology herein. For instance, single-channel vibration datasets were previously collected on the first 6 spans (among 18 spans) of a bridge. It is previously known that the first 5 spans contain undamaged, and the 6<sup>th</sup> span contains damage features in the dataset. To diagnose the conditions of the remaining 12 spans via a DL model (that might potentially house similar types of damage), it is prominent to have a trained DL model on that damage-associated dataset. Yet, under given circumstances, the dataset suffers from class imbalance due to data scarcity (5 undamaged and 1 damaged dataset among a total of 6 datasets corresponding to 6 spans). To tackle this problem, GAN can be used to generate synthetic (artificial) data for the DL model to be trained effectively. This instance is illustrated in Fig. 3 and Fig. 4. Fig. 3 illustrates the vibration-based damage detection via the DL model. Fig. 4 illustrates the GAN enhanced vibration-based damage detection via the DL model. In fact, Scenario#1 to Scenario#5 shown in Fig. 2 describes enhancing the real damaged data with different ratios of synthetic damaged data. The introduction of different scenarios in Fig. 2 is to demonstrate the effect of the enhancement in the training dataset and the subsequent impact on the prediction results by the  $M_2$  on the unseen data. The next sections explain the  $M_1$  and  $M_2$  workflows.

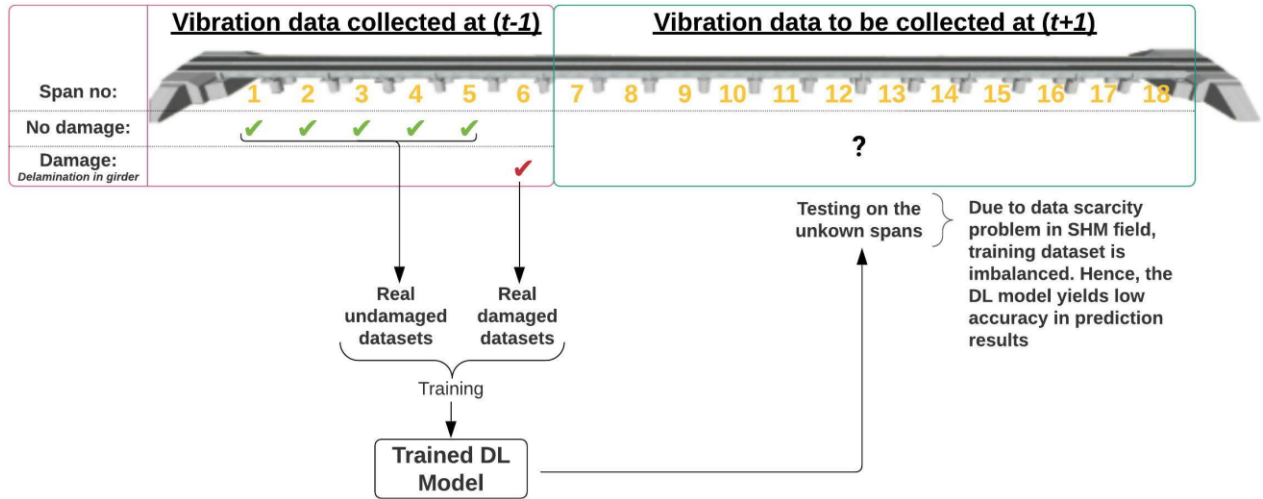


**Fig. 3.** Vibration-based damage detection via DL model

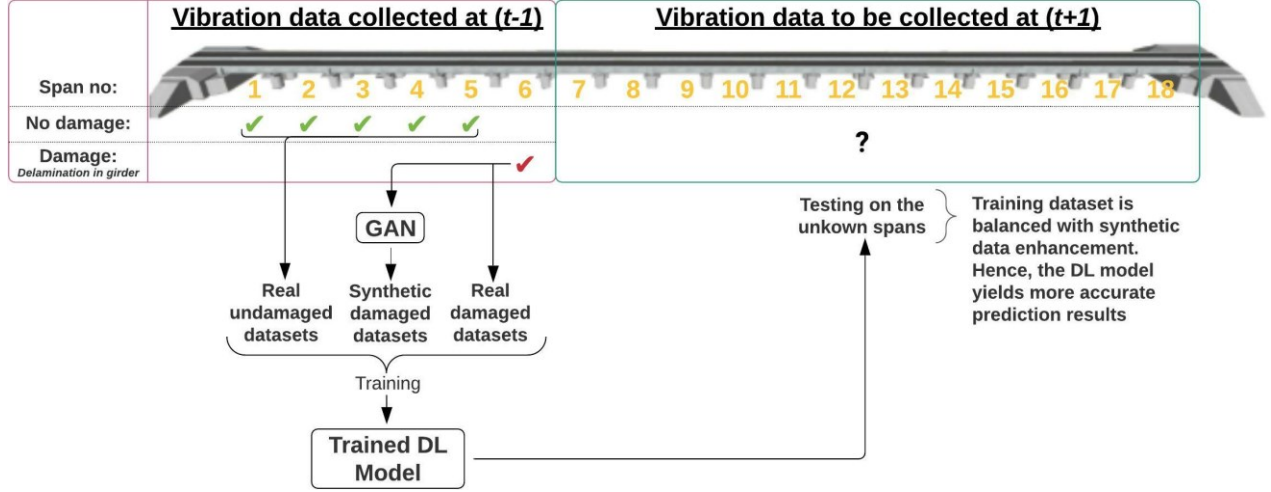


Fig. 4. GAN enhanced vibration-based damage detection via DL model

### 3) Workflow of 1-D WDCGAN-GP ( $M_1$ )

#### 3.1) $M_1$ - data preprocessing

Before the training of DL model, the standard practice in the DL field is to normalize the inputs on the same scale. Thus, the model can learn and predict more efficiently. During the model training, normalizing helps with the weights to be at the same scale. In other words, during the forward and backpropagation through the network where the dot products of the weights are computed, the normalization assist the model to perform accurate results and decrease processing time. In case the dataset has spikes, the normalization would help, otherwise, the spikes have a significant impact on the propagation because different levels of weight calculations can negatively affect the model quality during training. Yet, the dataset,  $[a_{11}]_{256}$ , does not possess large spikes. Also, the  $M_1$  consists of layers of batch and instance normalization which normalize the sampled batches during training. After a few training sessions of  $M_1$  with normalized input and unnormalized inputs, the results seemed that they are not distinctly different. In fact, it is observed that when the model is fed with the unnormalized data, it captures the spatial-temporal features in the dataset more effectively. Thus, normalization is not carried out before using the inputs for the  $M_2$ .

#### 3.2) $M_1$ – architecture

As a primary step, different options of layers and parameters are used in the architecture and the one with the best performance is selected. The used model architecture is illustrated in Fig. 5. The architecture takes the randomly given noise tensor ( $z$ ) and passes it through the five 1-D transpose convolutions. The first layer is  $filter = 64, stride = 2, padding = 0$ , then the rest of the layers are  $filter = 4, stride = 2, padding = 1$ . The batch normalization and ReLU is used after every layer except the last one. At the end of the generator part, Tanh activation function is used and consequently,  $[a_{11f}]_1$  is created. Then,  $[a_{11}]_1$  and  $[a_{11f}]_1$  are passed to the critic (the “discriminator” is named in WGAN “critic” as in their original paper) to be scored by the critic as to how real or fake each passed tensor is. Then the tensor passes through five 1-D convolutions. The first four layers are  $filter = 4, stride = 2, padding = 1$  and the layer is  $filter = 64, stride = 2, padding = 0$ . Leaky ReLU and dropout are used after the first layer. For the rest, instance normalization along with ReLU is used at the end of each layer.



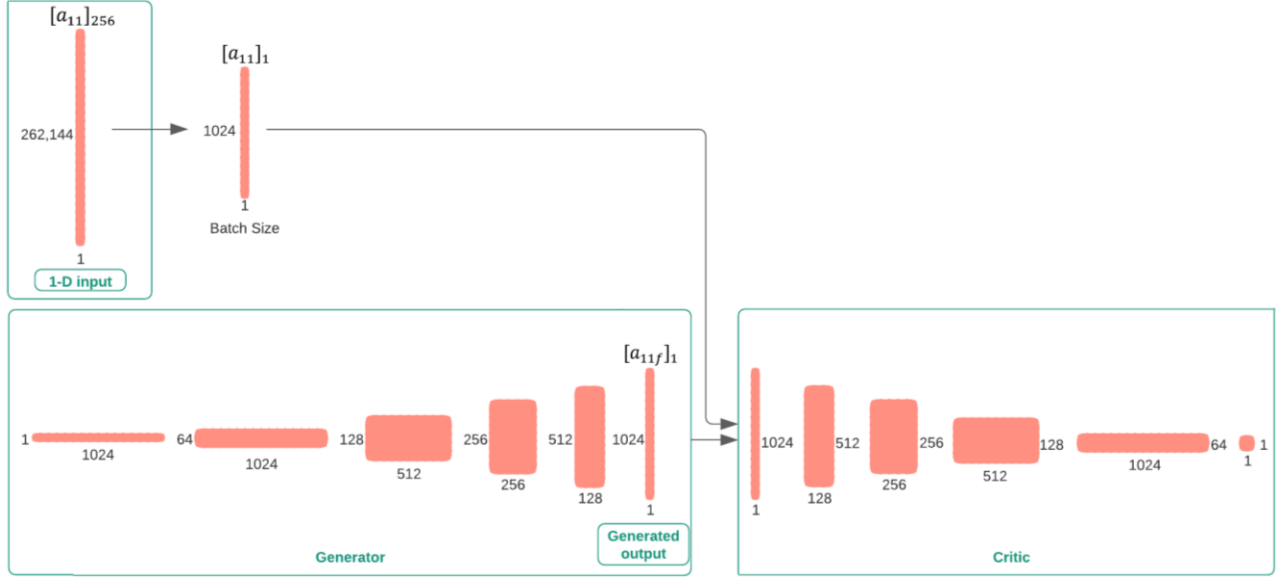


**Fig. 5.** 1-D WDCGAN-GP ( $M_1$ ) Architecture

### 3.3) $M_1$ - training and fine-tuning

As previously mentioned, the training phase of GAN is the most challenging part, and they are known in the DL community as the hardest model to train. Thus, it needs substantial effort during the fine-tuning process. Even though the model used in this paper is one of the most advanced GAN models, 1-D WDCGAN-GP, few approaches (so-called hacks) have been taken for the fine-tuning. After plenty of trials with different parameters in the model, using one layer of dropout with 70% in the critic is found very beneficial which avoids the overfitting and reduces the capacity of the critic and helps the model to reach the Nash equilibrium. Moreover, a random Gaussian noise is added that decays over each epoch (iteration). Thus, it gives handicap to the critic not to be superior to the generator. Consequently, the learning rate of  $5 \times 10^{-6}$  for generator and  $2 \times 10^{-5}$  for critic yielded the best result. The critic iterations, lambda parameter for the gradient penalty, and batch size are respectively picked as 12, 20, and 1024. The epoch number is used as 600 and took 44 hours of training. The AdamW optimizer is used in both the generator and critic for the optimization process. Lastly, the generator and critic loss functions are seemed to be converged at zero (Fig. 6) which is explained detailly in the next section.

### 3.4) $M_1$ - evaluation and interpretation

As training GAN are arguably the hardest ones among other DL models, evaluation of them could be very challenging as well. Unlike the other DL models, GAN does not have an objective function which makes it harder to evaluate the performance of the model. The evaluation of the GAN can be categorized as qualitative (manual evaluation) and quantitative where the former is based on visual, and the latter is based on the numerical evaluation. The widely used form of evaluation method of GAN is a qualitative approach that is visually evaluating the outputs of the generator in comparison with the training data, and the data is mostly in the form of images. However, this approach suffers from some drawbacks such as the limited number of generated outputs that can be viewed at a time by an observer and subjectivity being introduced from observers. Additionally, implementing this approach is not as effective as doing it on 1-D signal data. Therefore, several quantitative evaluation metrics are introduced to evaluate the performance of the model with no reached consensus in the DL as to which metric is the most effective. Because this study considers only nonparametric structural damage detection, the generated tensors (signals) are evaluated only in the time domain. In a study by Borji (2018) the evaluation methods of

GAN are investigated. One of the most used indicators for evaluating GAN is the Fréchet Inception Distance (FID) score [48] which is introduced as an improvement over Inception Score (IS) which is reported to be unable to capture the distribution of real and generated output. Also, several comparative studies proved its effectiveness against other GAN evaluation metrics. Particularly, FID showed very consistent performance when compared to the manual evaluation of the GAN outputs. The formula of FID is based on a statistical formulation that is shown in Equation 2.

$$FID(x, g) = \|\mu_x - \mu_g\|_2^2 + Tr(C_x + C_g - 2(C_x C_g)^{0.5}) \quad (2)$$

Where respectively the  $\mu_x$  and  $\mu_g$  are the means and  $C_x$  and  $C_g$  are the covariance matrices of real and generated signals and  $Tr$  is the trace of the matrices e.g., the sum of all the diagonal elements in the matrices. The lower the FID score, the more similar the compared data.

Another quantitative evaluation metric is introduced by [49] where the performance of GAN is evaluated on images based on three aspects: **Creativity**, **Inheritance**, and **Diversity**. These aspects are very significant for evaluating the GAN as they are expected to add creativity and diversity in the outputs as well as to keep the inheritance of the real input [50]. Among three, the Inheritance aspect is generally used for images where it shows how the generated images retain the key features of the real images such as texture. Therefore, it is not used in this presented study. The Creativity aspect indicates to what extent the generated outputs are not the exact ones of the real outputs (or dissimilar to each other) and the Diversity aspect indicates to what extent the generated outputs are similar to each other. The Creativity and Diversity computations are carried out by using Structural Similarity Index Measure (SSIM) [51] which was first used for image quality assessments by using similarity between the pixels of two images. If the SSIM of two images is 1, they are exactly the same; if the SSIM is 0, then they are entirely different images. The authors of the paper [49] defined a threshold value of 0.8 to calculate the creativity index; for instance, if the SSIM of generated and real data are higher than 0.8, they are concluded as duplicates. No threshold is used for the diversity index, but SSIM is employed between the generated datasets to compute the index. Using SSIM as an evaluation indicator is also used in [39] for evaluating the generated signals by GAN. There is no consensus on what SSIM values or thresholds should be used for creativity and diversity approaches for the evaluation of GAN. Intuitively, calculating SSIM of the generated outputs to real inputs indicates how creative the outputs are from the inputs. Calculating SSIM of the generated outputs to each other in the generated output dataset gives how diverse the outputs are from each other in the range of 0 between 1. The Creativity and Diversity indices are not directly used in this study, but SSIM computation is carried out to evaluate the extent of creativity and diversity of the generated outputs. As a result, in this study, the creative approach is investigated by computing SSIM between the generated and real tensors; the diversity approach is investigated by computing SSIM between the generated tensors within the generated dataset from the  $M_1$ . The SSIM equation is:

$$SSIM(x, g) = \frac{(2\mu_x\mu_g+c_1)(2\sigma_{xg}+c_2)}{(\mu_x^2+\mu_g^2+c_1)(\sigma_x^2+\sigma_g^2+c_2)} \quad (3)$$

In Equation (3)  $\mu_x$  and  $\mu_g$  are the means,  $\sigma_x$  and  $\sigma_g$  are the standard deviations, and  $\sigma_{xg}$  is the covariance of real data ( $x$ ) and generated data ( $g$ ). The  $c_1$  and  $c_2$  are the constants which are multiplication of  $k_1$  and  $L$ ; and  $k_2$  and  $L$  respectively, to stabilize the division with a weak denominator.  $L$  is the dynamic range of the signal and  $k_1$  and  $k_2$  are the constants which are picked in this study as  $1 \times 10^{-2}$  and  $3 \times 10^{-2}$ .

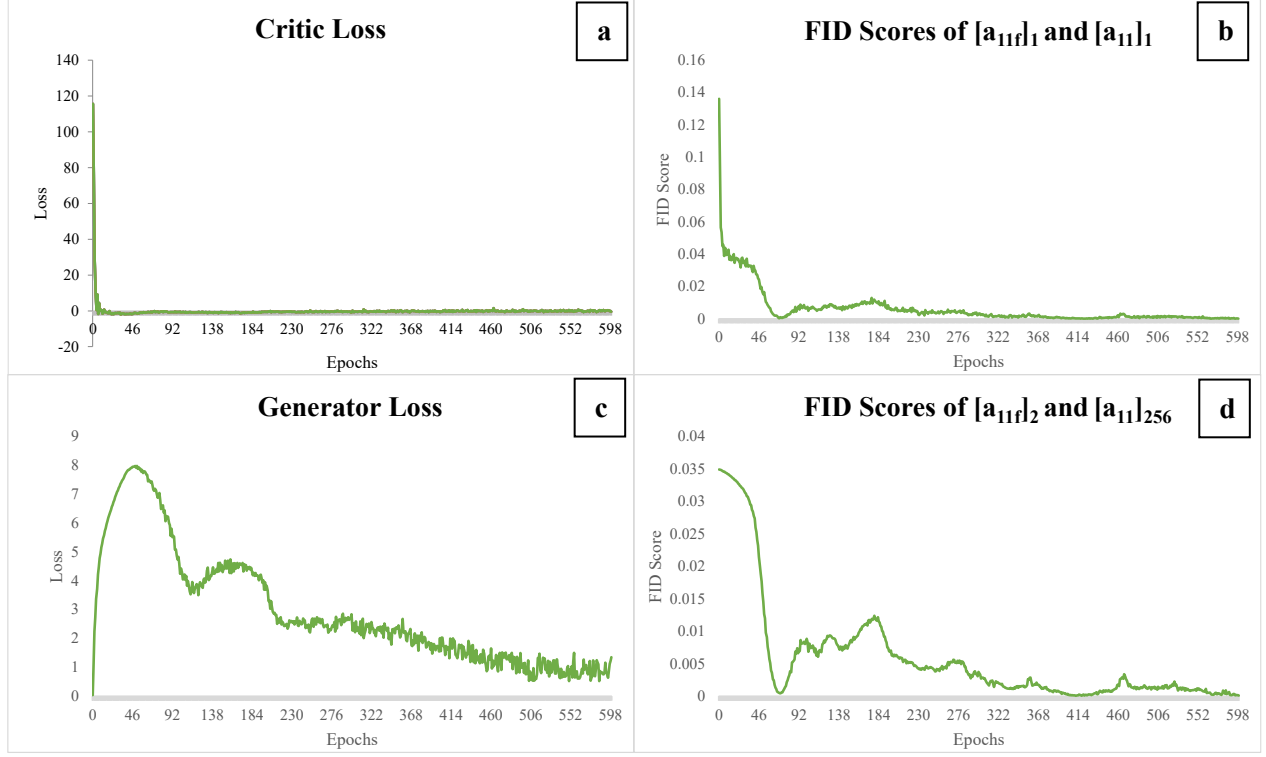


**Fig. 6.** Training plots of 1-D WDCGAN-GP ( $M_1$ )

During the training, the critic loss, the generator loss, and FID scores are monitored to observe the performance of the model (Fig. 6). It is noted that the critic loss is converged to zero. The generator loss on the other hand, which heuristically starts from near zero, then first increases since the critic has more knowledge of the real data domain and can easily guesses the generated outputs. After some epochs, the generator starts learning the gradients and generate more similar datasets. Hence, the generator loss seems to be returning to its first loss values which are expected for WDCGAN-GPs. The FID scores are monitored by computing the tensors between  $[a_{11f}]_1$  and  $[a_{11}]_1$  and they appear to be converging to zero. In other words, they are getting to look alike to each other (Fig. 6b and 6d). It is also important to note that the generated outputs,  $[a_{11f}]_1$ , are not only becoming similar to batched real data,  $[a_{11}]_1$ , but also to the entire raw signal data,  $[a_{11}]_{256}$ . The FID between  $[a_{11f}]_2$  and  $[a_{11}]_{256}$  is calculated during the training. It is found that the FID scores of  $[a_{11f}]_1$  and  $[a_{11}]_1$  and the FID scores of  $[a_{11f}]_1$  and  $[a_{11}]_{256}$  are both converging to zero with the same trend over the epochs. This reveals that batch sampling from the raw data,  $[a_{11}]_{256}$ , in shuffle mode, does not produce different results since it suggests that the 262,144 sized raw datasets have repetitive features in a particular time length. Hence, it validates using the batch samples of 1-second tensors (1024 samples in each tensor) in this study. Note that since the aim of this study is nonparametric damage detection, which is not based on any parameters but directly on raw data, the order of the samples in the batch sampled tensors is irrelevant. Batch sampling in shuffle mode also helps the training of the model in a way that it converges faster, preventing bias, and preventing learning the order of the data. Therefore, for simplicity, in the rest of the study, only the calculations between batch sampled generated and real datasets ( $[a_{11f}]_1$  and  $[a_{11}]_1$ ) are considered. Furthermore, in Fig. 6, it is observed that the FID score of  $[a_{11f}]_1$  between  $[a_{11}]_1$  are started from 0.136 and decreased to  $1.5 \times 10^{-5}$ , which is a reduction of 9060 times. This large reduction shows that the model learned the dataset thoroughly and can generate very similar datasets. The FID scores can depend on various factors (model architecture and hyperparameters and used dataset) as to how much it reduced, or where it started and ended. To better comprehend the FID values, in one study by [52], the authors

compared their GAN model to others on MNIST data (image dataset of handwritten numbers) and the FID score was decreased by 6 times during the training. In another study, the resulting decrease in FID score was found around 85 [53]. Although a decrement of 9060 times can be looking like a success, it might also be an indication of overfitting which will be investigated in the following paragraph.

After the  $M_1$  is trained, the FID scores are computed between the real and generated tensors,  $[a_{11}]_1$  and  $[a_{11f}]_1$ . Then, the Probability Density Function (PDF) is plotted of the calculated FID scores (Fig. 5). It is seen that the FID scores are dense around the value of  $7 \times 10^{-4}$ . The purpose of visualizing the PDF is to comprehend the variance of FID values. Although during the training it went down to  $1.5 \times 10^{-5}$ , the variance of the FID scores could have been extending to a value of 0.10 as well, which in this case it could be concluded that the model did not learn. However, as seen in Fig. 7, the variance is considerably low along with very low FID values, 194 times lower than the starting point of 0.1359.

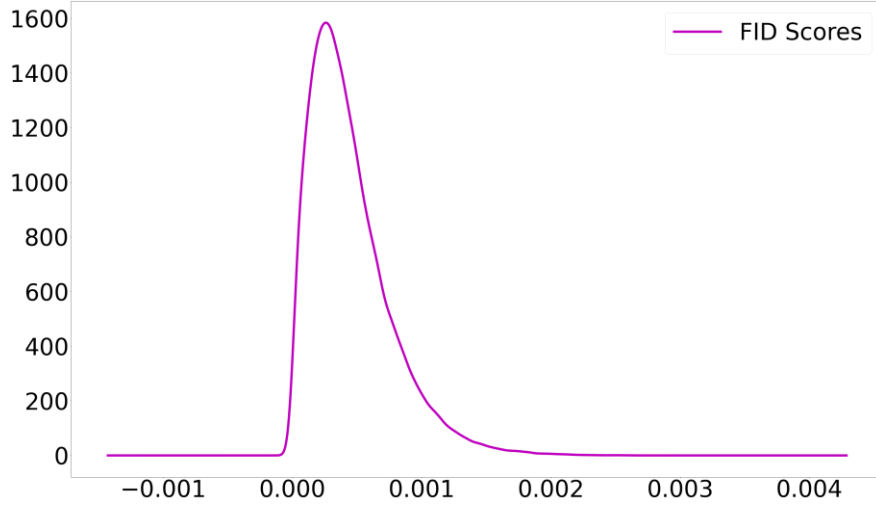


**Fig. 7.** Probability Density Function plot of FID Scores

Next, the creativity and diversity approaches are investigated. For that, the SSIM between the  $[a_{11f}]_1$  and  $[a_{11}]_1$ , and SSIM within the  $[a_{11f}]_1$  are computed respectively. The PDFs of the creativity and diversity results are plotted in Fig. 8. The SSIM values do not go beyond the 0.8 threshold value, and they are dense around the value of 0.3 which may be concluded that the generated tensors are not the exact copies of the real tensors. Yet, further validations are needed to support this claim since SSIM was used only once in the literature for 1-D data generation [39]. Thus,  $M_1$  can generate creative outputs. The creativity measure also determines the overfitting of the model; considering that the resulting value is small, it can be concluded that the model is not overfitted in the training dataset since no exact copies exist. The diversity values are dense around the value of 0.36 and it can be stated that the generated tensors are not alike to each other. This can mean that diversity exists within the generated tensors. Based on the creativity and diversity aspects of the generated dataset, none of the generated and real tensors is the exact copies of each other and none of the generated tensors is exact copies of each other.

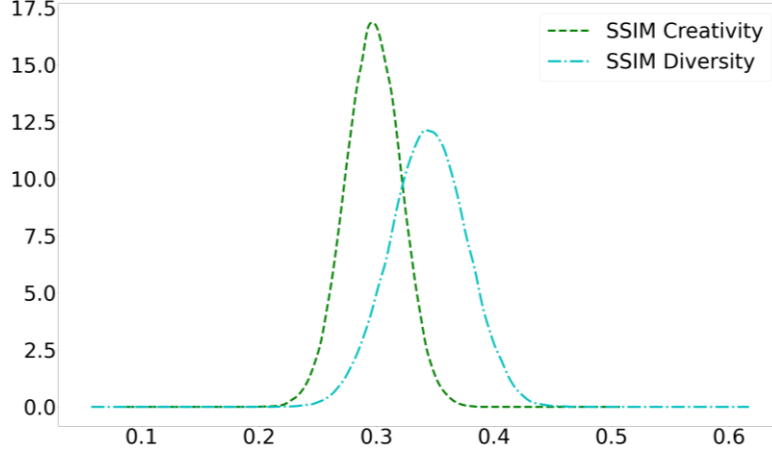


**Fig. 8.** Probability Density Function plots of Creativity and Diversity by using SSIM

Two pairs of vibration tensors two from real and two from the generated dataset are boxes plotted in Fig. 9 to visualize and compare the statistical meanings. The plotted tensors are picked as one pair has the lowest FID, and one pair has the lowest FID score. The boundaries of boxes and size of whiskers are looking alike along with the mean and median values. The box plots show that the statistical meanings and distributions of the generated and real data pairs are very similar to each other.

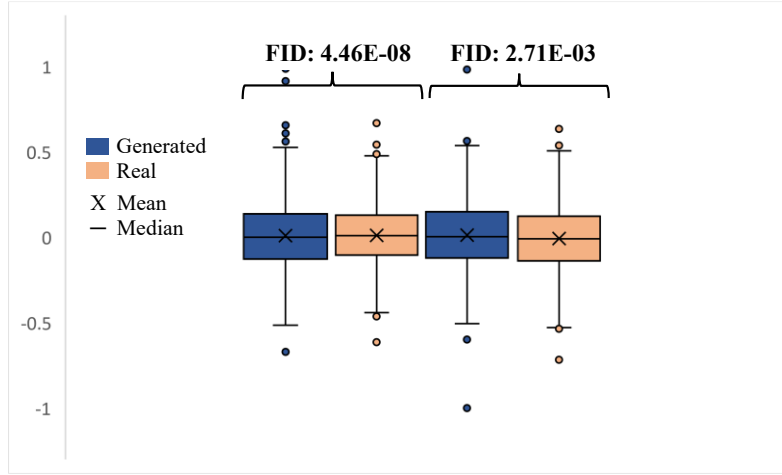


**Fig. 9.** Box plots of the tensors with lowest and highest FID values

Lastly, qualitative evaluation is implemented on the real input and generated outputs of  $M_1$ . As previously mentioned, qualitative evaluation is the most preferred method for image data, 2-D data, yet it has drawbacks for evaluating 1-D data. The same vibration tensors that were used in Fig. 9 are plotted in Fig. 10. Although it is difficult to determine the similarity between the generated and the real data as in image-based applications, the plotted tensor pairs in Fig. 10 reveal good consistency throughout the sample length for the lowest and highest FID score ones. Although the generated tensors have some eye-catching spikes, the 1-D DCNN ( $M_2$ ) model's predictions were successful, which is explained in section 4.4.

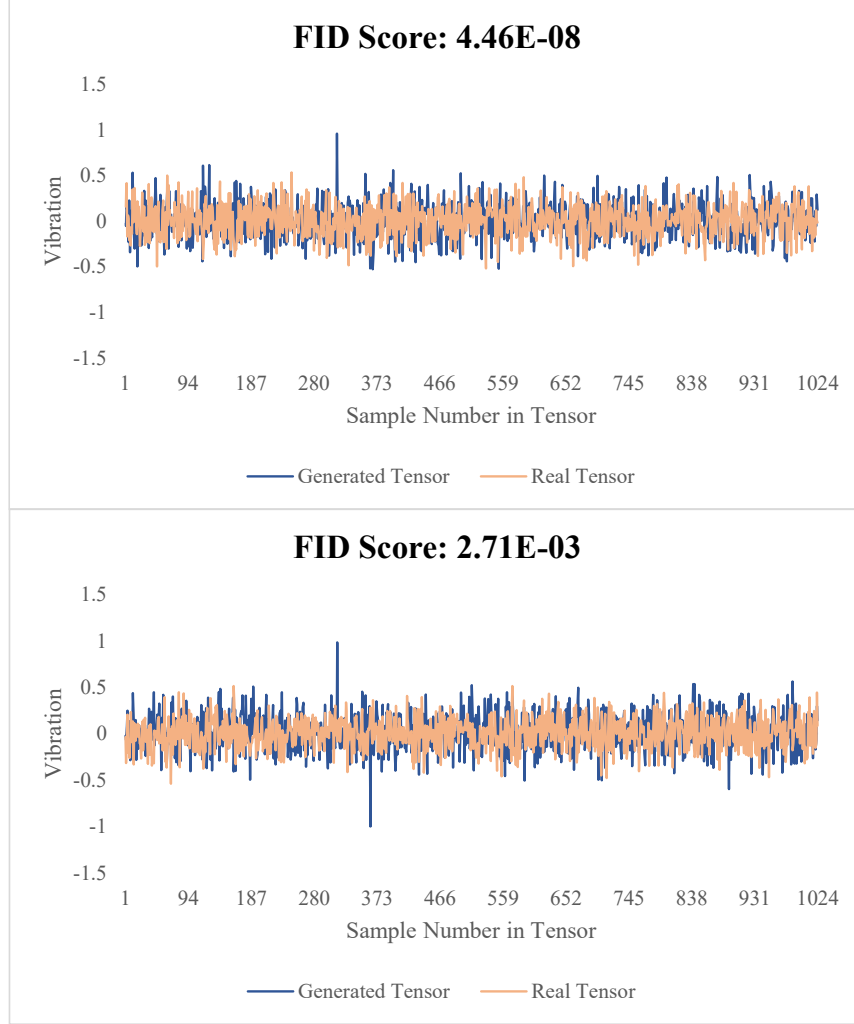


**Fig. 10.** Tensor pairs with lowest and highest FID values

#### 4) Workflow of 1-D DCNN ( $M_2$ )

##### 4.1) $M_2$ - data processing

Before feeding the tensors in the  $M_2$  (1-D DCNN), the tensors are normalized in the range of -1 and +1. Subsequently, the generated tensors from  $M_1$  and batch sampled tensors from the  $[a_{11}]_{256}$  are randomly extracted into the data pool. Then, the datasets are arranged to be used for each different scenario as stated in Fig. 2.

##### 4.2) $M_2$ - architecture

The same critic architecture used in  $M_1$  is utilized for  $M_2$  with adding a sigmoid function at the end of the  $M_2$  in order to produce a prediction score for each tensor (the critic network in  $M_1$  had no activation function at the end of the last layer and only realness or fakeness scores were processed). The sigmoid function produces prediction scores in the range of 0 to 1 where 0 denotes undamaged and 1 denotes damaged tensor. Also, unlike in the critic network of  $M_1$ , no dropout is used in  $M_2$  since it is not considered as necessary for a simple detection process. Lastly, the test or validation loss indicators are not



plotted in this study since the prediction results for the unseen data which is presented in section 4.4 demonstrated that the model can successfully classify the tensors.

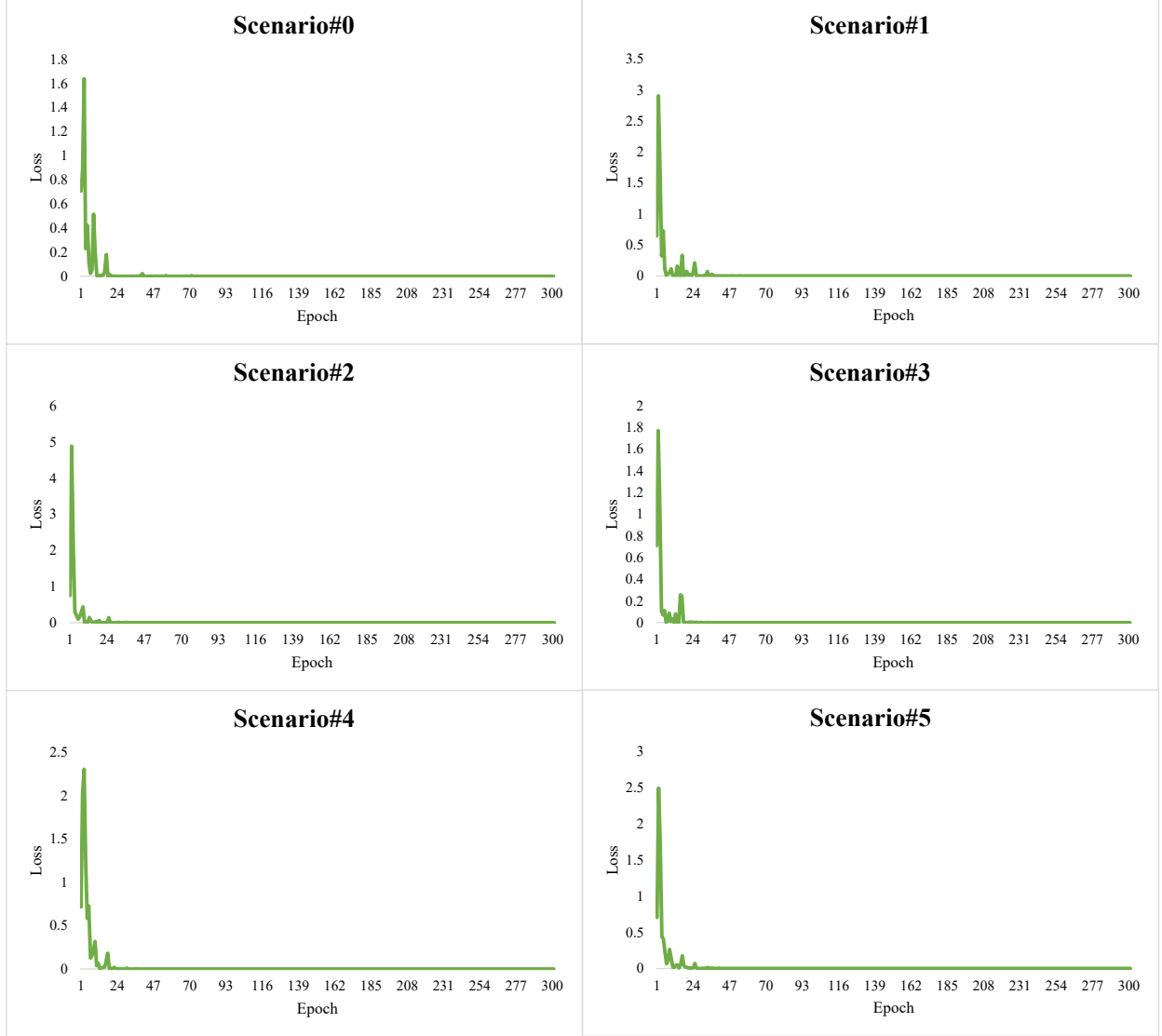


**Fig. 11.** Training plots of  $M_2$  (1-D DCNN) for each scenario

#### 4.3. $M_2$ – training and fine-tuning

After several trials of using different hyperparameters in the  $M_2$ , the learning rate for the Scenario#0, Scenario#1, and Scenario#2 is chosen as  $8 \times 10^{-4}$  and for the rest of the scenarios, it is  $3.5 \times 10^{-3}$ . The batch size and number of the epoch is picked as 30 and 300, respectively. Also, Cross-Entropy is used as the loss function which was not used in  $M_1$ . Finally, the training loss functions are plotted in Fig. 11 which is seemed to be converged at zero axis for all scenarios, in other words, the model learned the training dataset. Then, the model is tested on the unseen tensors for each scenario and yielded successful results which are explained in detail in the following section.

#### 4.4) $M_2$ - evaluation and interpretation

Regardless of how the model learned the training dataset successfully, the testing phase determines the performance of the model (testing dataset contains instances that the model did not see before, in other words, **unseen** data instances). Additionally, the success of the model on the unseen data indicates if the model is overfitted to the training data and cannot generalize to other datasets.

The test results are evaluated by using one regression two classification metrics. The reason why a regression metric is used on a classification problem is to measure the error on faulty predictions. In a simple vibration-based damage detection problem in SHM, a prediction score such as 0.77 can be both interpreted as damaged data (with a threshold assumption of 0.5 and converting into the label of “1” which indicates damage data) and the quantification of the damage data (such as loosening a bolt not 100% but with a percentage of 77). Therefore, it is prominent to distinguish between two indications. The **Mean Absolute Error (MAE)** is used as the regression metric:

$$MAE = \frac{\sum_{i=1}^n |y_i - x_i|}{n} \quad (4)$$

Where  $n$  is the total number of samples,  $i$  is the index of sample,  $y$  is the predicted value, and  $x$  is the actual value of the sample. MAE metric is also used for many regression and classification tasks in both ML and DL studies. For the classification metrics, **Classification Accuracy (CA)** and **Average Precision (AP)** scores are utilized. The CA is one of the most used metrics in ML and DL studies that simply measures the total correct predictions over total predictions:

$$Classification\ Accuracy = \frac{Number\ of\ correct\ predictions}{Total\ number\ of\ predictions} \quad (5)$$

In order to use the CA, a threshold has to be assigned in the domain of prediction scores to convert prediction score into the closest label (in this study the used labels are “0” undamaged and “1” damaged). This study used 0.50 as the threshold. The prediction scores made at 0.50 and above are converted to 1 and the others are to 0. Yet, evaluating a model based on one threshold value can be misleading about the performance of the model. The AP is one of the most used metrics which gives average precision at all possible thresholds, especially employed for benchmarking different DL models on various datasets. It is a very useful metric to compare different models’ successes without specifying a decision threshold. The AP combines and summarizes the **precision** and **recall** curve into one value which represents the weighted summation of precisions at the different thresholds. The weight is defined as the increase in recall from each succeeding threshold. The precision is the ratio of true positive over the sum of true positive and false positive. This metric implies the frequency of correct predictions at every prediction; thus, it reflects how reliable the model is in predicting the samples as positive. The recall is the ratio of true positive over the sum of true positive and false negative which implies the model’s ability to classify positive samples and only interests in how the positive samples are classified. Briefly, the AP is the area under the precision-recall curve. An area of 1.0 means that the classifier is a perfect model and 0.5 means the classifier is a poor model. The formulation of AP can be shown as:

$$AP = \sum_n [Recall(n) - Recall(n - 1)] \times Precision(n) \quad (6)$$

After  $M_2$  made the predictions on the unseen (test) dataset which each scenario consists of 30 samples as given in Fig. 2, the results including the ground truths and prediction scores are bar plotted in Fig. 12. Also, the **MAE**, **CA**, and **AP** metrics are computed and displayed on the top right corner of the bar plots for each scenario in Figs. 12-17. At first glance, one can catch the close prediction scores to ground truths (actual labels) in these figures. Yet with a closer look, there are few incorrect prediction results. Starting with Scenario#0, the regression and classification metrics show that the model predicts with 100% CA,

1.00 AP, and  $4.7 \times 10^{-3}$  MAE. That means the model yields consistent results on every tensor with no inaccurate classification. Note that Scenario#0 (no synthetic tensor is involved) was created as a “reference” scenario for benchmarking purposes. For the rest of the scenarios, from Scenario#1 to Scenario#5, the inclusion ratio of the number of synthetic tensors in the damage test dataset is gradually decreased. This change slightly impacted the classification results. Firstly, the corresponding scenarios in Figs. 13-17 includes one incorrect prediction on different tensors that are circled in red color. While the  $M_2$  is more confident in its predictions in Scenario#1-2-3, for Scenario#4 and Scenario#5 it remains uncertain on a few tensors. The incorrect predictions caused the MAE metric to increase about 6.5 times from  $4.7 \times 10^{-3}$  to  $0.3 \times 10^{-1}$  ranges when comparing **Scenario#0** to **other scenarios**. This indicates that the predictions of  $M_2$  include more errors for the other scenarios than the reference scenario. Having one incorrect prediction caused the CA to score decrease from 100% to 97%, while the AP score is decreased from 1.00 to 0.97 only for Scenario#1 and Scenario#2. The change in AP score is basically the result of the high confidence of the model on the data for Scenario#1 and Scenario#2. Since the model is very sure of its predictions, the AP score always contains one incorrect prediction at every threshold value unless the threshold is selected very close to 0 or 1. While the inclusion of synthetic tensors slightly changed the MAE metric, the CA and AP metrics experienced a negligible amount of decreases which is critical for vibration-based damage detection. The classification metric is more used for the level-1 damage diagnostics (damage detection) and the error metrics can be more beneficial for the level-2 damage diagnostics (damage quantification) since the damage quantification is carried out based on the errors. Hence, considering one incorrect prediction out of 30 predictions for Scenario#1-5, the prediction results on the test dataset can be concluded as excellent.

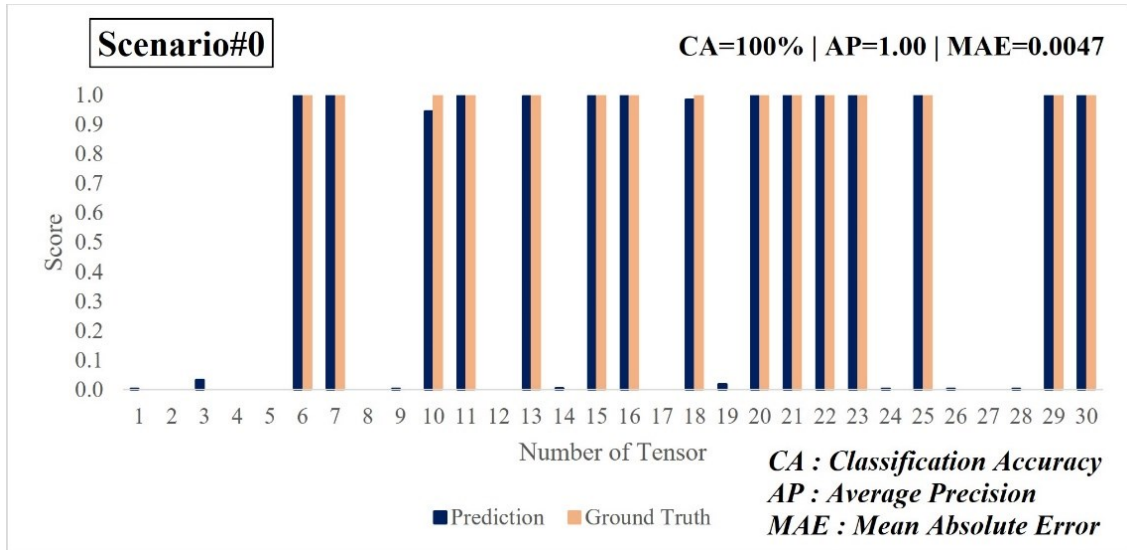


**Fig. 12.** Testing results of  $M_2$  for Scenario#0

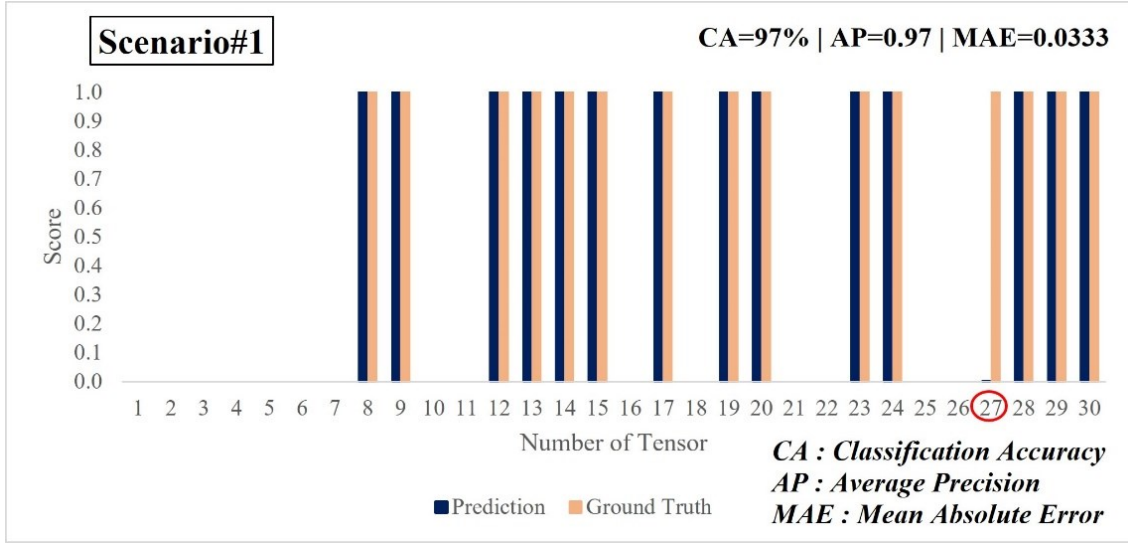


**Fig. 13.** Testing results of  $M_2$  for Scenario#1

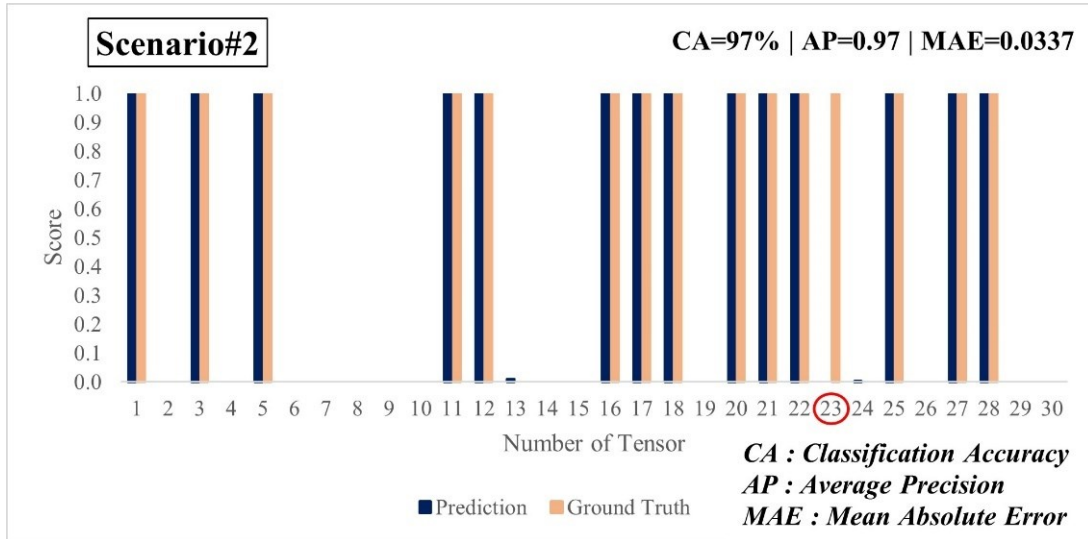


**Fig. 14.** Testing results of  $M_2$  for Scenario#2

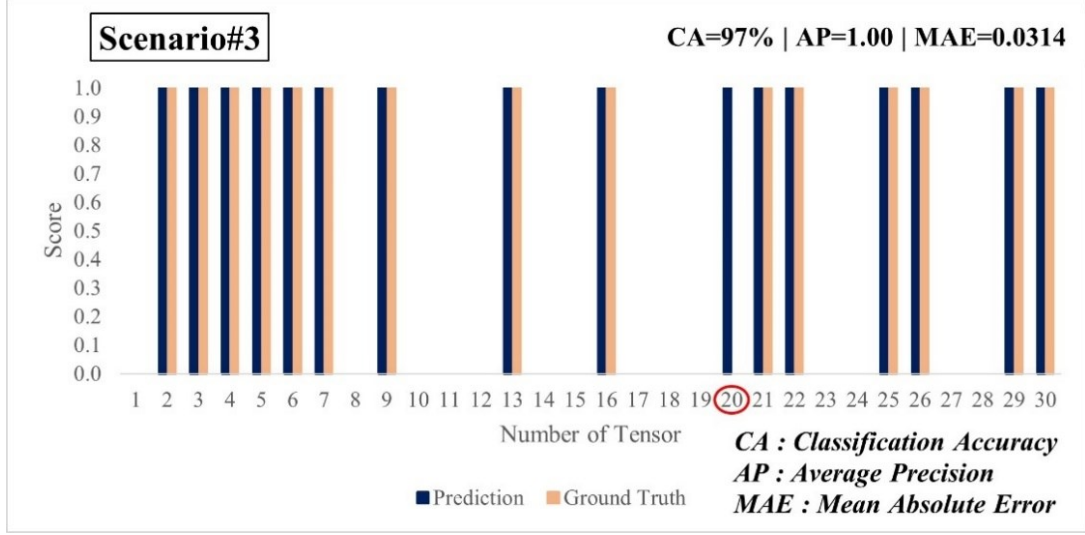


Fig. 15. Testing results of  $M_2$  for Scenario#3

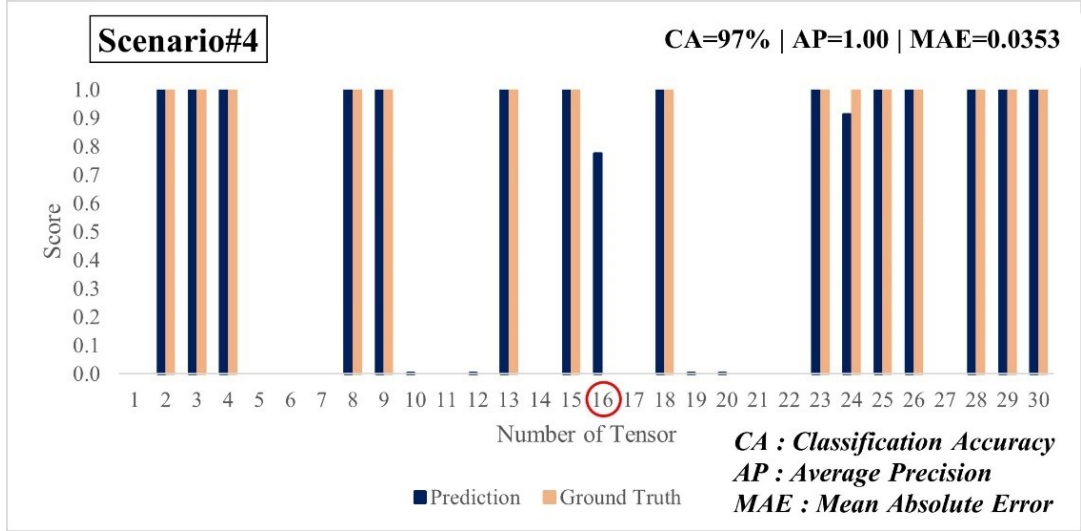


Fig. 16. Testing results of  $M_2$  for Scenario#4

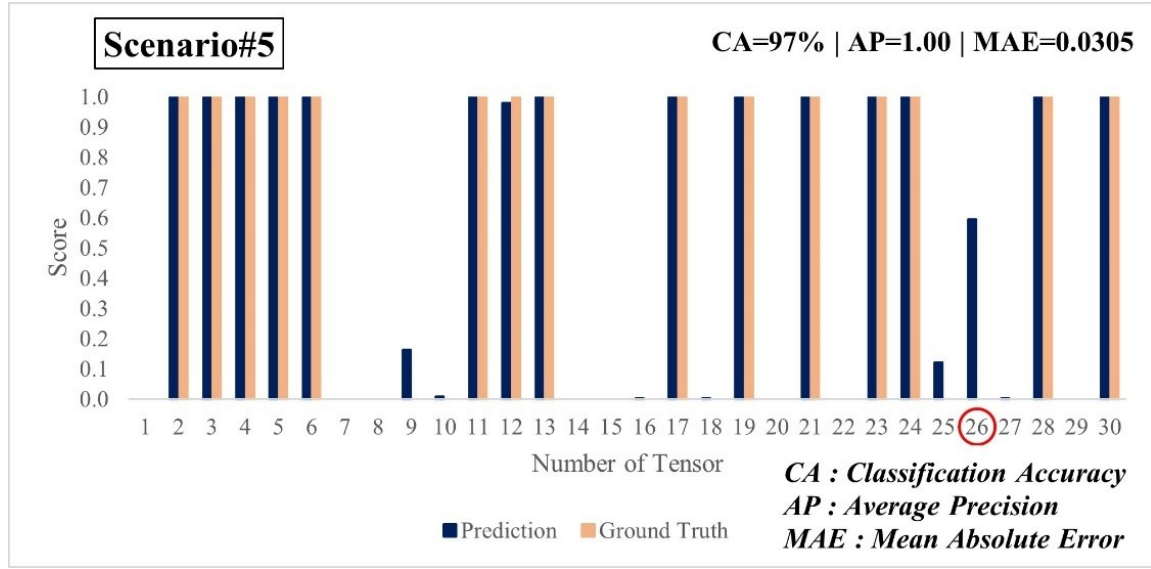


Fig. 17. Testing results of  $M_2$  for Scenario#5

## 5) Summary and conclusions

Damage diagnostics on civil structures can be very expensive and time-consuming since obtaining vibration data that includes damage features is challenging. The scarcity of data hinders the use of AI methods. Recently, the researchers took advantage of AI methods such as ML and DL algorithms for vibration-based structural damage diagnostics and they produced excellent results. Particularly the DL methods perform exceptionally well, yet it requires a large amount of data to operate. This study utilized **One Dimensional Wasserstein Deep Convolutional Generative Adversarial Networks using Gradient Penalty (1-D WDCGAN-GP)** to generate synthetic vibration data and validated the generated datasets with quantitative and qualitative methods. Then, six different scenarios are created to reflect the real-life scenarios that may be faced in SHM of a structure for the purpose of vibration-based damage detection. Each of these scenarios includes different levels (ratios) of synthetic vibration tensors mixed with real vibration tensors in the training dataset. Then, for each scenario, the 1-D DCNN model is employed to perform damage detection on the raw vibration tensors. The 1-D DCNN is trained on the varying ratios of synthetically enhanced training dataset; then tested on the unseen real dataset. The prediction results are evaluated with regression and classification metrics. While the prediction scores for the synthetically enhanced dataset scenarios yielded **97% classification accuracy**, the real dataset yielded **100% classification accuracy**. In other words, when the DCNN is trained with GAN enhanced damaged class and real undamaged class, its prediction capability falls in **3% error margin** compared to the benchmark case, Scenario#0. Thus, from the perspective of DCNN model, the enhanced damaged class is almost indistinguishable from the real damaged datasets. The main conclusions of this study can be listed as the following:

- GAN can be used to tackle the imbalanced data that is caused by the data scarcity in SHM of civil structures, which is a well-known problem in the field. Imbalanced data classes can be detrimental to ML and DL based structural damage detection applications. By generating synthetic datasets with GAN, the training dataset can be balanced. Thus, this increases the efficiency of damage diagnostics applications.



- Additional research is needed for level-1 damage diagnostics (detection) and level-2 damage diagnostics (quantification) using GAN. Since damage detection is based on classification metrics and damage quantification is based on error metrics, new studies should investigate the effect of data enhancement with GAN on the precision of quantification of structural damages. Also, further developments and investigations are necessary for evaluating the GAN-generated vibration signals since the existing evaluation methodologies consider image (2-D) data.
- Consequently, the proposed methodology and framework in this study open the door for the implementation of more ML and DL tools to be used in vibration-based structural damage diagnostics for civil structures since this study demonstrated that GAN can be used to generate synthetic datasets to reduce the needing for data collection.

### Data availability statement

Vibration data used in this study was made available in Abdeljaber et al., 2017. Some or all used models, codes, and detailed results are available from the corresponding author of this paper upon request.

### Acknowledgement

The authors would like to thank members of the CITRS (Civil Infrastructure Technologies for Resilience and Safety) Research Initiative at the University of Central Florida. The second author would like to acknowledge the support of the National Aeronautics and Space Administration (NASA) Award No. 80NSSC20K0326 and by the U.S. National Science Foundation (NSF) Division of Civil, Mechanical and Manufacturing Innovation (grant number 1463493).

### Nomenclature

The following symbols are used in this paper:

Symbol	Description
$[a_{01}]_{256}$	Vibration data at joint#1 in undamaged scenario (0) in raw form (256 seconds)
$[a_{11}]_{256}$	Vibration data at joint#1 in damaged scenario (1) in raw form (256 seconds)
$[a_{11}]_1$	Vibration tensor at joint#1 in damaged scenario (1) in batched form (1 second)
$[a_{01}]_1$	Vibration tensor at joint#1 in undamaged scenario (0) in batched form (1 second)
$[a_{11f}]_1$	Generated, “fake”, vibration tensor from GAN which the model is trained on $[a_{11}]_{256}$
$M_1$	Used 1-D WDCGAN-GP model in the paper
$M_2$	Used 1-D DCNN model in the paper

### References

1. Das S, Saha P, Patro SK (2016) Vibration-based damage detection techniques used for health monitoring of structures: a review. Journal of Civil Structural Health Monitoring. <https://doi.org/10.1007/s13349-016-0168-5>
2. Avci O, Abdeljaber O, Kiranyaz S, Hussein M, Gabbouj M, Inman DJ (2021) A review of vibration-based damage detection in civil structures: From traditional methods to Machine Learning and Deep Learning applications. Mechanical Systems and Signal Processing 147:107077

3. Dong C-Z, Catbas FN (2021) A review of computer vision–based structural health monitoring at local and global levels. *Structural Health Monitoring*. <https://doi.org/10.1177/1475921720935585>
4. Gul M, Catbas FN (2008) Ambient Vibration Data Analysis for Structural Identification and Global Condition Assessment. *Journal of Engineering Mechanics*. [https://doi.org/10.1061/\(ASCE\)0733-9399\(2008\)134:8\(650\)](https://doi.org/10.1061/(ASCE)0733-9399(2008)134:8(650))
5. Yin T, Lam HF, Chow HM, Zhu HP (2009) Dynamic reduction-based structural damage detection of transmission tower utilizing ambient vibration data. *Engineering Structures*. <https://doi.org/10.1016/j.engstruct.2009.03.004>
6. Krishnan Nair K, Kiremidjian AS (2007) Time Series Based Structural Damage Detection Algorithm Using Gaussian Mixtures Modeling. *Journal of Dynamic Systems, Measurement, and Control*. <https://doi.org/10.1115/1.2718241>
7. Gul M, Catbas FN (2011) Damage Assessment with Ambient Vibration Data Using a Novel Time Series Analysis Methodology. *Journal of Structural Engineering*. [https://doi.org/10.1061/\(ASCE\)ST.1943-541X.0000366](https://doi.org/10.1061/(ASCE)ST.1943-541X.0000366)
8. Silva M, Santos A, Figueiredo E, Santos R, Sales C, Costa JCWA (2016) A novel unsupervised approach based on a genetic algorithm for structural damage detection in bridges. *Engineering Applications of Artificial Intelligence*. <https://doi.org/10.1016/j.engappai.2016.03.002>
9. Alom MZ, Taha TM, Yakopcic C, Westberg S, Sidike P, Nasrin MS, Hasan M, van Essen BC, Awwal AAS, Asari VK (2019) A State-of-the-Art Survey on Deep Learning Theory and Architectures. *Electronics*. <https://doi.org/10.3390/electronics8030292>
10. González MP, Zapico JL (2008) Seismic damage identification in buildings using neural networks and modal data. *Computers & Structures*. <https://doi.org/10.1016/j.compstruc.2007.02.021>
11. Lee J, Kim S (2007) Structural Damage Detection in the Frequency Domain using Neural Networks. *Journal of Intelligent Material Systems and Structures*. <https://doi.org/10.1177/1045389X06073640>
12. Cury A, Crémona C (2012) Pattern recognition of structural behaviors based on learning algorithms and symbolic data concepts. *Structural Control and Health Monitoring*. <https://doi.org/10.1002/stc.412>
13. Lee JJ, Lee JW, Yi JH, Yun CB, Jung HY (2005) Neural networks-based damage detection for bridges considering errors in baseline finite element models. *Journal of Sound and Vibration*. <https://doi.org/10.1016/j.jsv.2004.01.003>
14. Santos A, Figueiredo E, Silva MFM, Sales CS, Costa JCWA (2016) Machine learning algorithms for damage detection: Kernel-based approaches. *Journal of Sound and Vibration*. <https://doi.org/10.1016/j.jsv.2015.11.008>
15. Bandara RP, Chan TH, Thambiratnam DP (2014) Structural damage detection method using frequency response functions. *Structural Health Monitoring*. <https://doi.org/10.1177/1475921714522847>

16. Ghiasi R, Torkzadeh P, Noori M (2016) A machine-learning approach for structural damage detection using least square support vector machine based on a new combinational kernel function. *Structural Health Monitoring*. <https://doi.org/10.1177/1475921716639587>
17. Abdeljaber O, Avci O (2016) Nonparametric Structural Damage Detection Algorithm for Ambient Vibration Response: Utilizing Artificial Neural Networks and Self-Organizing Maps. *Journal of Architectural Engineering*. [https://doi.org/10.1061/\(ASCE\)AE.1943-5568.0000205](https://doi.org/10.1061/(ASCE)AE.1943-5568.0000205)
18. Pathirage CSN, Li J, Li L, Hao H, Liu W, Ni P (2018) Structural damage identification based on autoencoder neural networks and deep learning. *Engineering Structures*. <https://doi.org/10.1016/j.engstruct.2018.05.109>
19. Shang Z, Sun L, Xia Y, Zhang W (2021) Vibration-based damage detection for bridges by deep convolutional denoising autoencoder. *Structural Health Monitoring*. <https://doi.org/10.1177/1475921720942836>
20. Rastin Z, Ghodrati Amiri G, Darvishan E (2021) Unsupervised Structural Damage Detection Technique Based on a Deep Convolutional Autoencoder. *Shock and Vibration*. <https://doi.org/10.1155/2021/6658575>
21. Abdeljaber O, Avci O, Kiranyaz S, Gabbouj M, Inman DJ (2017) Real-time vibration-based structural damage detection using one-dimensional convolutional neural networks. *Journal of Sound and Vibration*. <https://doi.org/10.1016/j.jsv.2016.10.043>
22. Yu Y, Wang C, Gu X, Li J (2019) A novel deep learning-based method for damage identification of smart building structures. *Structural Health Monitoring*. <https://doi.org/10.1177/1475921718804132>
23. Avci O, Abdeljaber O, Kiranyaz S, Inman D (2017) Structural Damage Detection in Real Time: Implementation of 1D Convolutional Neural Networks for SHM Applications. [https://doi.org/10.1007/978-3-319-54109-9\\_6](https://doi.org/10.1007/978-3-319-54109-9_6)
24. Abdeljaber O, Avci O, Kiranyaz MS, Boashash B, Sodano H, Inman DJ (2018) 1-D CNNs for structural damage detection: Verification on a structural health monitoring benchmark data. *Neurocomputing*. <https://doi.org/10.1016/j.neucom.2017.09.069>
25. Eren L (2017) Bearing Fault Detection by One-Dimensional Convolutional Neural Networks. *Mathematical Problems in Engineering*. <https://doi.org/10.1155/2017/8617315>
26. Iwana BK, Uchida S (2021) An empirical survey of data augmentation for time series classification with neural networks. *PLOS ONE* 16:e0254841
27. GARDNER P, BARTHORPE RJ (2019) On Current Trends in Forward Model-driven SHM. *Structural Health Monitoring* 2019. <https://doi.org/10.12783/shm2019/32351>
28. Goodfellow IJ, Pouget-Abadie J, Mirza M, Xu B, Warde-Farley D, Ozair S, Courville A, Bengio Y (2014) Generative Adversarial Networks.
29. Goodfellow I (2016) NIPS 2016 Tutorial: Generative Adversarial Networks.

30. Salimans T, Goodfellow I, Zaremba W, Cheung V, Radford A, Chen X (2016) Improved Techniques for Training GANs.
31. Radford A, Metz L, Chintala S (2015) Unsupervised Representation Learning with Deep Convolutional Generative Adversarial Networks.
32. Arjovsky M, Chintala S, Bottou L (2017) Wasserstein GAN.
33. Gulrajani I, Ahmed F, Arjovsky M, Dumoulin V, Courville A (2017) Improved Training of Wasserstein GANs.
34. Truong T, Yanushkevich S (2019) Generative Adversarial Network for Radar Signal Synthesis. 2019 International Joint Conference on Neural Networks (IJCNN). <https://doi.org/10.1109/IJCNN.2019.8851887>
35. Kuo P-H, Lin S-T, Hu J (2020) DNAE-GAN: Noise-free acoustic signal generator by integrating autoencoder and generative adversarial network. International Journal of Distributed Sensor Networks. <https://doi.org/10.1177/1550147720923529>
36. Luo T, Fan Y, Chen L, Guo G, Zhou C (2020) EEG Signal Reconstruction Using a Generative Adversarial Network With Wasserstein Distance and Temporal-Spatial-Frequency Loss. Frontiers in Neuroinformatics. <https://doi.org/10.3389/fninf.2020.00015>
37. Wulan N, Wang W, Sun P, Wang K, Xia Y, Zhang H (2020) Generating electrocardiogram signals by deep learning. Neurocomputing. <https://doi.org/10.1016/j.neucom.2020.04.076>
38. Wang T, Trugman D, Lin Y (2021) SeismoGen: Seismic Waveform Synthesis Using GAN With Application to Seismic Data Augmentation. Journal of Geophysical Research: Solid Earth. <https://doi.org/10.1029/2020JB020077>
39. Sabir R, Rosato D, Hartmann S, Guhmann C (2021) Signal Generation using 1d Deep Convolutional Generative Adversarial Networks for Fault Diagnosis of Electrical Machines. 2020 25th International Conference on Pattern Recognition (ICPR). <https://doi.org/10.1109/ICPR48806.2021.9413119>
40. Shao S, Wang P, Yan R (2019) Generative adversarial networks for data augmentation in machine fault diagnosis. Computers in Industry. <https://doi.org/10.1016/j.compind.2019.01.001>
41. Guo Q, Li Y, Song Y, Wang D, Chen W (2020) Intelligent Fault Diagnosis Method Based on Full 1-D Convolutional Generative Adversarial Network. IEEE Transactions on Industrial Informatics. <https://doi.org/10.1109/TII.2019.2934901>
42. Gao S, Wang X, Miao X, Su C, Li Y (2019) ASM1D-GAN: An Intelligent Fault Diagnosis Method Based on Assembled 1D Convolutional Neural Network and Generative Adversarial Networks. Journal of Signal Processing Systems. <https://doi.org/10.1007/s11265-019-01463-8>
43. Zhang X, Qin Y, Yuen C, Jayasinghe L, Liu X (2021) Time-Series Regeneration with Convolutional Recurrent Generative Adversarial Network for Remaining Useful Life Estimation.
44. Zhang C, Kuppannagari SR, Kannan R, Prasanna VK (2018) Generative Adversarial Network for Synthetic Time Series Data Generation in Smart Grids. 2018 IEEE International Conference on

- Communications, Control, and Computing Technologies for Smart Grids (SmartGridComm). <https://doi.org/10.1109/SmartGridComm.2018.8587464>
45. Jiang H, Wan C, Yang K, Ding Y, Xue S (2021) Continuous missing data imputation with incomplete dataset by generative adversarial networks–based unsupervised learning for long-term bridge health monitoring. *Structural Health Monitoring*. <https://doi.org/10.1177/14759217211021942>
  46. Fan G, Li J, Hao H, Xin Y (2021) Data driven structural dynamic response reconstruction using segment based generative adversarial networks. *Engineering Structures*. <https://doi.org/10.1016/j.engstruct.2021.111970>
  47. Borji A (2018) Pros and Cons of GAN Evaluation Measures.
  48. Heusel M, Ramsauer H, Unterthiner T, Nessler B, Hochreiter S (2017) GANs Trained by a Two Time-Scale Update Rule Converge to a Local Nash Equilibrium.
  49. Guan S, Loew M (2019) Evaluation of Generative Adversarial Network Performance Based on Direct Analysis of Generated Images. In: 2019 IEEE Applied Imagery Pattern Recognition Workshop (AIPR). IEEE, pp 1–5
  50. Guan S, Loew M (2020) A Novel Measure to Evaluate Generative Adversarial Networks Based on Direct Analysis of Generated Images.
  51. Wang Z, Bovik AC, Sheikh HR, Simoncelli EP (2004) Image Quality Assessment: From Error Visibility to Structural Similarity. *IEEE Transactions on Image Processing*. <https://doi.org/10.1109/TIP.2003.819861>
  52. Costa V, Lourenço N, Correia J, Machado P (2019) COEGAN. *Proceedings of the Genetic and Evolutionary Computation Conference*. <https://doi.org/10.1145/3321707.3321746>
  53. MITCSAIL (2019) Spatial Evolutionary Generative Adversarial Networks. In: <https://jamaltoutouh.github.io/downloads/GECCO-2019-Mustangs.pdf>.